Axial compressive performance of laminated bamboo column with aramid fiber reinforced polymer

Zhen Wang[1,2], Haitao Li[1,2*], Benhua Fei[2], Mahmud Ashraf[1,3], Zhenhua Xiong[4], Rodolfo Lorenzo[5], Changhua Fang[2]

[1] College of Civil Engineering, Nanjing Forestry University, Nanjing 210037, China;

[2] Department of Biomaterials, International Centre for Bamboo and Rattan, No. 8, Futong East Street, Chaoyang District, Beijing 100102, China

[3] School of Engineering, Deakin University, Geelong Waurn Ponds, VIC 3216, Australia.

[4] Ganzhou Sentai bamboo company LTD, Ganzhou 341001, China.

[5] University College London, London WC1E 6BT, UK.

*Corresponding author: Haitao LI, Professor, E-mail: lhaitao1982@126.com

ABSTRACT

This paper presents test results obtained from an experimental investigation to check the feasibility of reinforcing laminated bamboo columns by using aramid fiber reinforced polymer (AFRP) composites and to examine the effect of slenderness ratio on AFRP reinforced columns. Eighteen full-scale columns were grouped into 6 slenderness categories including 3 specimens without AFRP reinforcements. Obtained results were used to study the effect of AFRP on failure modes, ultimate load carrying capacities and displacements for columns with carrying slenderness ratios. The use of AFRP reinforcements had obvious effects on failure modes. Existing relevant analytical models were used to check their suitability in predicting compression resistance of the considered columns but obtained comparisons showed significant room for improvement. Two equations are proposed herein, based on experimental evidence, to predicted the ultimate load carrying capacity of AFRP reinforced laminated bamboo columns. The proposed equations showed good agreement with test results.

KEYWORDS

Aramid fiber; Laminated bamboo; Compression; Composite materials; Reinforcing

1 INTRODUCTION

Use of bamboo and engineered bamboo products are increasingly recognized as viable alternatives for traditional construction materials in sustainable development of future cities and communities as they could potentially reduced the effects of climate change through sustainable consumption and production. Use of bamboo and engineered bamboo can also support in mitigating poverty in some parts of the world, which is one of the 17 Sustainable Development Goals (SDG) [1] recommended by the United Nations. Although small diameter and natural variation in mechanical properties of bamboo hinder its wider usage in construction, engineered bamboo products such as laminated bamboo lumber (LBL) (see Fig. 1), parallel bamboo strand lumber (PBSL) and glue laminated bamboo (glubam) could potentially lead to enormous opportunities for bamboo products to be used in all types of building construction [2][3][4]. Engineered bamboo products are reported to provide resistances that are often higher than their timber counterparts [5], and in many cases are

superior to concrete or steel in terms of strength-to-weight ratio. Strength of engineered bamboo products could be enhanced by using fiber reinforced polymer (FRP) to produce innovative hybrid composite materials. The current research presents an investigation on the effect of using aramid fiber reinforced polymer (AFRP) wraps around LBL columns.

Although research on FRP reinforced bamboo composites is still in its infancy, previously reported investigations on FRP reinforced wood products has recently been reported by Wang et al. [6]. In the earlier stages of FRP-timber composites research, the focus was mainly on timber beams. Plevris and Triantafillou [7] carried out tests to study the effect of reinforcing fir wood with carbon fiber reinforced polymers (CFRP) and concluded that addition of even very small area fractions of reinforcement could result in significant improvement of the mechanical properties. Sonti et al. [8] added 3% of pultruded glass/vinylester FRP by volume to yellow-poplar glulam and obtained an 18% increase in stiffness in addition a 26% increase in strength. Vahedian et al. [9] reported that stiffness of strengthened timber beams with FRP attached to the tensile area increased between 31% and 64%. More recently, research on timber columns reinforced with fiber reinforced polymers has increased. Taheri et al. (2009) studied the effect of reinforcing glulam columns with carbon or glass fibers and found that fiber composites have a positive impact on the compressive strength of the columns. With the gradual development of bamboo products, some researches turned their focus into fiber reinforced bamboo. Wei et al. [10] confirmed that mechanical properties of bamboo scrimber beams could be improved by using FRP. Lv and Liu [11] strengthened laminated bamboo beams with single or double layers of basalt fiber reinforced polymer (BFRP) sheet and reported an increase of 14% and 24% in the ultimate load for single and double layers, respectively.

Among available engineered bamboo products, laminated bamboo structural components, provide eco-friendly (less adhesive) and statistically more uniform alternatives, while maintaining beneficial attributes of bamboo such as aesthetic appeal and ease of handling. Considerable research on different aspects of laminated bamboo including processing, performance, and economical considerations have been reported in literature [12]-[20]. Compression performance is one of the key aspects in structural engineering and, hence, researchers reported buckling behavior of original bamboo culms [21][22][23]. Lv [24] investigated the mechanical performance of five groups of the GluBam column with a cross-section of 56 mm × 56 mm and evaluated the influence of the slenderness ratio on the ultimate load. Li et al. [25] carried out tests to investigate the relationship between the slenderness ratio and load-carrying capacity of laminated bamboo columns and proposed design equations based on obtained experimental evidence.

To the author's knowledge, studies considering the performance of laminated bamboo columns reinforced with fiber composites are non-existent, or at best scarce. This lack of knowledge gave rise to the present investigation, with the aim of studying the behavior of full-scale structural members with FRP laminates both experimentally and analytically.

2 EXPERIMENTAL PROGRAM

2.1 Materials

The test material was side press laminated bamboo produced by Sentai Bamboo and Wood Co., Ltd., Jiangxi Province in China. With resorcinol as adhesive, laminated bamboo was made of bamboo strips (with a section of 7 × 21 mm) glued together by hot pressing at 157 °C for about 15 min under main pressure of 9 MPa, side pressure of 6.5 MPa, as shown in Fig. 1. Fifteen specimens were divided into 5 groups of 3 specimens based on the length of columns, wrapped with aramid fiber reinforced polymer (AFRP) sheets. Lengths of specimens ranged from 600 mm to 3000 mm. It is worth noting that three identical laminated bamboo columns without AFRP with a height of 3000 mm were also used as control specimens. Table 1 lists designations and other geometric properties of the specimen groups. The size of the column section was 100 × 100 mm, with four chamfers of 10 mm, as shown in Fig. 2. Chamfers were adopted for easy adhesion of AFRP sheets to substrates. The fiber direction of the composite sheet was along the length of the column. In addition, both ends of the columns were wrapped by additional composite sheets with a length of 50 mm to prevent the ends from

premature cracking due to the proximity of support reactions (see Fig. 2b).

2.2 Compression testing procedure

The displacement for the mid-height deflection of two adjacent faces was measured by two Laser Displacement Sensors with a TDS-540 data logger. Two strain gauges were pasted on each middle side surface of the specimens, as shown in Fig. 3. The monotonic load was applied along the longitudinal axis of the column ensuring that the geometric center of the column section and the test machine were aligned on the same vertical line. Specimens were subjected to preloading five times prior to loading until the vertical strain value of four faces were comparable to each other to ensure that the specimen was in a state of axial compression.

3 DISCUSSION ON TEST OBSERVATIONS

3.1 Failure mechanism

3.1.1 Failure mode

At the initial loading stage, the specimen was in a linear elastic state without obvious lateral deflection. But the failure phenomena of columns with different slenderness ratios were distinctly divergent. Short columns failed due to strength showing complete failure of the column section and was characterized by considerable ductility prior to failure. While the slender columns predominantly buckling failure and no obvious local damages were observed. Typical load-displacement and load-deflection responses are shown in Fig. 4 and 5, respectively.

The failure of AA600-2 was dominated by the compressive strength completely since no lateral deflection was observed during the loading process. As the force increased, the upper end of the column crushed and the extra reinforced fibers ruptured, which is shown in Fig. 6a. AA600-3 gradually bent after the elastic stage and the deflection at midspan increased rapidly. During the bending process, audible crackling sounds resulted from fracture of aramid fibers. Once columns reached their peak load, a loud brittle fracture sound was heard prior to the flexural failure of bamboo laminae, which was followed by gradual expansion of main cracks. At this stage, the load of the column dropped to 80% or even lower of the ultimate load. No evident deflection was observed at the cross-sections near column ends. AA600-1 showed the same phenomena as AA600-3 did at the beginning of the plastic stage, but it did not crush at the mid height eventually.

The failure modes of specimens in the AA1100 and AA1700 series were comparable to each other. Load-displacement responses of AA1100 and AA1700 were somewhat similar to AA600 series but the columns showed much larger lateral displacement when compared to those observed for AA600. However, the end sections showed some lateral displacement at the initiation of the plastic stage. Before the onset of failure, the column bent and the upper and lower hinges tilted abruptly. Afterwards, a fracture occurred in the middle of the specimen, and the force dropped sharply.

The load-displacement response of AA2300 series was characterized by a brief plastic plateau and small lateral deflections. Then the column bent and the upper and lower hinges tilted abruptly. Afterward, a fracture occurred in the middle of the specimen, and the bearing capacity dropped sharply. No fracture occurred to the specimen, and the column could almost restore to its configuration before the test.

The failure phenomena and the load-displacement behavior of AA3000 and control columns (without AFRP wraps) were quite similar to that of AA2300 columns, except for the popup of the column accompanied by a loud noise at the end of the experiment. No fracture occurred to the specimen of the AA3000 series. However, splitting of bamboo laminae was observed in the control series and cracks extended along the length of the column.

3.1.2 Failure influenced region

Failures predominantly occurred at the mid-height of the column specimens, as shown in Fig. 6b. For short columns, e.g. AA600-3, the end was more prone to cracking (see Fig. 6c) as the compression resistance was much higher than

longer specimens and local failures occurred due to excessive stress at the ends. However, failure was eventually triggered due to local bending at mid-height as lateral displacement gradually increased. In addition to the fracture of the composite sheet and bamboo laminae, some debonding between the composite sheet and bamboo laminae was observed.

Contrary to the wrapped column, the crevice of columns without the composite sheet propagated from the end to the middle of the specimen (Figs. 6e and 6f).

The fact that the location of the fracture was not necessarily at the glue layer of the bamboo laminae indicated that the bond performance of the laminated bamboo was good enough. In addition, the bamboo nodes or joints were not the weak points of the laminated bamboo columns as the fracture did not occur specifically at the bamboo nodes or joints.

3.1.3 Failure procedure

The typical failure procedure of the composite column under compression loading can be divided into 2 or 3 stages as illustrated in Fig. 7. For AA600, AA1100 and AA1700 specimens, it is considered that the process of strain accumulation could be described as three stages, i.e., the initial elastic stage, the intensifying stage and the failure stage. But the failure process of AA2300, AA3000 and control specimens was relatively unambiguous, which was characterized by an elastic stage followed by a brief plastic stage.

As illustrated in Fig. 7, the compressive strains of one or two surfaces were transformed into tensile strain before the final failure of the specimen. During the initial stages of loading, all column sections were uniformly compressed, and the load-strain response were linear. As the load gradually increased, column suffered lateral deflections, predominantly at mid-height. When the load increased to about 80% to 90% of the ultimate load, the compressive strain of the surface along the bending direction began to deviate and finally converted to tensile strain (for AA1100 and AA1700 series). After the load reached the peak value, the compressive strain value of the surface under compression increased rapidly.

3.1.4 Failure mechanism analysis

Fig. 8 shows comparison of load-displacement responses for all column series considered in the current study. Comparing the load-displacement behaviors of the AA3000 and the control group, it may be concluded that the AFRP wrapping increased the load carrying capacity and deformability of the laminated bamboo columns and consequently leading to the improvement in ductility. It is worth noting that the extra wraps at the column ends were effective in preventing splitting observed in control specimens.

The slenderness ratio played a significant role in AFRP wrapped bamboo laminate column behavior as expected. The compression failure of the column could transform from plastic failure to brittle failure with an increasing slenderness ratio. Both load carrying capacity and axial displacement decreased as the slenderness ratio increases (Fig. 8). However, the lateral deflection of mid-span rose rapidly as the column length increased from 600 mm to 1 700 mm (Fig. 5).

It is worth noting that the lateral displacements observed in laminated bamboo columns were mostly oriented in the radial direction of bamboo strips. Even though the column sections were square in cross-section, a weak axis appeared due to the geometric size and mechanical properties of the bamboo strips. Furthermore, a distinct difference in the failure mechanism between the AA1700 and AA2300 series has been noticed, which may be due a shift from local failure to global failure; this phenomenon is discussed further in Section 3.3.

3.2 Analysis of compression behavior

3.2.1 Influence of AFRP on column resistance

Test results obtained for the control and AA3000 series are shown in Table 2. Addition only 0.77% of AFRP by volume resulted an increase of 13% in strength and 10% in stiffness of the laminated bamboo columns. However, AA3000 columns failed due to global buckling and the AFRP did not show any failure demonstrating its potential to be more effective for less slender columns. For AA1700, the deflection was larger, resulting in a better utilization of FRP and a

better reinforcement effect. For AA600 and 1100 columns, AFRP sheets were even more effective by providing better confinement for laminated bamboo strips making them ductile in nature.

3.2.1 Influence of slenderness ratio

Table 3 shows that the ultimate load, displacement, compressive strength, and ultimate strain were decreasing with the increasing of the slenderness ratio.

3.3 Analytical investigations

Suppose a column with a bending stiffness of EI is unable to move in the horizontal direction under axis compression, due to the elastic constraint of both ends connected with other components. As the end section can turn slightly, the bending moment at the column end is proportional to the rotation angle. Fig. 9 shows a schematic showing a column (of length l) is subjected to end moments (M_A and M_B) and rotations (ω_A and ω_B), which depend on the proportionality coefficients c_A and c_B (kN·mm/rad) respectively.

The column shall remain in equilibrium in the form of micro-bending under the critical force F_{cr}. The relationships between the couple moment of the support reaction M_A and M_B, and the rotation angle of both ends ω_A and ω_B are:

$$M_A = c_A(+\omega_A),\ M_B = c_B(-\omega_B) \tag{1}$$

The horizontal support reaction values at both ends are $\frac{M_B - M_A}{l}$.

The bending moment at any cross section of the column can be obtained as follows:

$$M(x) = F_{cr}\omega - M_A - (M_B - M_A)\frac{x}{l} \tag{2}$$

Thus, the approximate differential equation of the deflection curve of the compression element is:

$$EI\omega'' = -M(x) = -F_{cr}\omega + M_A + (M_B - M_A)\frac{x}{l} \tag{3}$$

After simplifying and introducing parameters $k^2 = F_{cr}/EI$, Equation (3) becomes

$$\omega'' + k^2\omega = k^2\left(\frac{M_A}{F_{cr}} + \frac{M_B - M_A}{F_{cr}}\frac{x}{l}\right) \tag{4}$$

The general solution of the differential equation is

$$\omega = A\sin kx + B\cos kx + \frac{M_A}{F_{cr}} + \frac{M_B - M_A}{F_{cr}}\frac{x}{l} \tag{5}$$

And its first derivative is:

$$\omega' = Ak\cos kx - Bk\sin kx + \frac{M_B - M_A}{F_{cr}l} \tag{6}$$

The undetermined constants A, B, and unknown constants M_A, M_B, shall be determined by boundary conditions.

A lower support A: $x = 0$, $\omega = 0$, $\omega' = \frac{M_A}{c_A}$, and hence

$$B = -\frac{M_A}{F_{cr}},\ A = \frac{1}{k}\left[\frac{-(M_B - M_A)}{F_{cr}l} + \frac{M_A}{c_A}\right] \tag{7}$$

Substituting the constants A, B into Equations (5) and (6) give rise to the following expressions:

$$\omega=\frac{1}{k}\left(-\frac{M_B-M_A}{F_{cr}l}+\frac{M_A}{c_A}\right)\sin kx-\frac{M_A}{F_{cr}}\cos kx+\frac{M_A}{F_{cr}}+\frac{M_B-M_A}{F_{cr}}\frac{x}{l} \tag{8}$$

and

$$\omega'=\frac{1}{k}\left(-\frac{M_B-M_A}{F_{cr}l}+\frac{M_A}{c_A}\right)\cos kx+\frac{M_A}{F_{cr}}k\sin kx+\frac{M_B-M_A}{F_{cr}l} \tag{9}$$

Then, the followings can be obtained from Equations (8) and (9) by using the boundary conditions at the upper support B: $x=l$, $\omega=0$, $\omega'=-\frac{M_B}{c_B}$.

$$\frac{1}{k}\left(-\frac{M_B-M_A}{F_{cr}l}+\frac{M_A}{c_A}\right)\sin kl-\frac{M_A}{F_{cr}}\cos kl+\frac{M_A}{F_{cr}}+\frac{M_B-M_A}{F_{cr}}=0 \tag{10}$$

and

$$\left(-\frac{M_B-M_A}{F_{cr}l}+\frac{M_A}{c_A}\right)\cos kl+\frac{M_A}{F_{cr}}k\sin kl+\frac{M_B-M_A}{F_{cr}l}+\frac{M_B}{c_B}=0 \tag{11}$$

The above two equations can be regarded as a system of linear algebraic equations with two unknown quantities M_A and M_B.

$$\left[\left(\frac{1}{kl}+\frac{1}{kc_A/F_{cr}}\right)\sin kl-\cos kl\right]M_A+\left(1-\frac{1}{kl}\sin kl\right)M_B=0 \tag{12}$$

$$\left[\left(\frac{1}{kl}+\frac{1}{kc_A/F_{cr}}\right)k\cos kl+k\sin kl-\frac{1}{l}\right]M_A+\left(\frac{1}{l}+\frac{1}{c_B/F_{cr}}-\frac{1}{l}\cos kl\right)M_B=0 \tag{13}$$

If $kl=u$, $c_A/F_{cr}=\overline{c_A}$, $c_B/F_{cr}=\overline{c_B}$. In order to obtain non-zero solutions of M_A and M_B from the above two formulas, the following determinant must be equal to zero.

$$\begin{vmatrix} \left[\left(\frac{1}{u}+\frac{l}{u\overline{c_A}}\right)\sin u-\cos u\right] & \left(1-\frac{1}{u}\sin u\right) \\ \left[\left(\frac{1}{u}+\frac{l}{u\overline{c_A}}\right)\frac{u}{l}\cos u+\frac{u}{l}\sin u-\frac{1}{l}\right] & \frac{1}{l}+\frac{l}{\overline{c_B}}-\frac{1}{l}\cos u \end{vmatrix}=0 \tag{14}$$

After simplifying,

$$\left(\frac{1}{c_A}+\frac{1}{c_B}\right)\left(\frac{\sin u}{u}-\cos u\right)+\frac{l}{uc_Ac_B}\sin u+\frac{1}{l}\left(2-2\cos u-u\sin u\right)=0 \tag{15}$$

In each specific case, the minimum non-zero solution shall be obtained from Equation (15) by c_A and c_B. Then the critical load of columns can be predicted by using Formula (16) with $u=kl$,

$$F_{cr}=\frac{u^2EI}{l^2} \tag{16}$$

The Euler column formula for the critical force of the compressive column can be obtained by substituting the minimum non-zero solution of u.

In the current research, both ends of the column have the same proportional coefficient, i.e. $c_A=c_B$, so Equation (15) can be simplified as follows:

$$\left[\left(\frac{l}{c_A}+\frac{l}{c_B}+\frac{l}{c_A}\times\frac{l}{c_B}\right)\frac{1}{u}-u\right]\sin u-\left(\frac{l}{c_A}+\frac{l}{c_B}+2\right)\cos u+2=0 \tag{17}$$

Taking the precise test values of AA1700-1 into Equation (17), i.e. $l=1700$ mm and

$\overline{c_A} = \overline{c_B} = \frac{c_A}{F_{cr}} = \frac{c_B}{F_{cr}} = \frac{M_A}{F_{cr}\omega_A} = \frac{M_B}{F_{cr}\omega_B} = 301$ mm , then $u = 4.483$.

Thus, the Euler column formula for the critical force at present work is

$$F_{cr} = \frac{4.483^2 EI}{l^2} = \frac{\pi^2 EI}{(0.7l)^2} \tag{18}$$

So, the effective length of the column in the current study is $0.7l$.

The calculation formulas for the slenderness ratio of the column are given as:

$$\lambda = l_0 / r \tag{19}$$

$$r = \sqrt{I / A} \tag{20}$$

Where l_0 is the calculated length of the column, r is the section radius of gyration, I is the section moment of inertia, and A is the section area, which is 9800 mm^2 for the plain column and 9875 mm^2 for the reinforced column. The moment of inertia I for the plain column can be calculated as:

$$I = \int_A y^2 dA = 2\int_{40}^{\frac{h}{2}} y^2 \times 2x dy + 2\int_0^{40} y^2 \times 2x dy = 4\int_{40}^{50} y^2 (90 - y) dy + 4\int_0^{40} y^2 \times 50 dy = 7.9 \times 10^6 \,\text{mm}^4 \tag{21}$$

In the case of reinforced composite columns, the transformed critical moment of inertia for the columns with FRP (calculated by multiplying every dimension parallel to the axis of bending by the modular ratio of composite to bamboo), shall be determined by Equations (22) and (23).

$$y_t = \frac{\sum A_i y_i}{\sum A_i} \tag{22}$$

$$I = \sum \left[I_i + A_i \left(y_t - y_i \right)^2 \right] \tag{23}$$

Where A_i is the transformed cross-sectional area of each constituent laminate, i; y_i is the distance of the centroidal axis of each constituent from the datum; and I_i are the moment of inertia of each laminate. The transformed critical moment of inertia is calculated to be 8.1 × 10^6 mm^4.

3.4 Theoretical calculations

3.4.1 Euler column formula

Columns fail by buckling when their critical load is reached. Long columns shall be analyzed with the Euler column formula shown in Equation (24):

$$P_{cr} = \frac{n^2 \pi^2 EI}{l^2} \tag{24}$$

Where P_{cr} is the allowable load, n is the factor accounting for the end conditions, E is the modulus of elasticity, I is the moment of inertia, and l is the length of the column. $n = 1$ as the column was pivoted in both ends at present work.

However, the Euler column formula can only be applied to the column whose slenderness ratio is higher than the critical value λ_p which shall be calculated by Equation (25).

$$\lambda_p = \pi \sqrt{\frac{E}{\sigma_p}} \tag{25}$$

Where σ_p is the proportional limit. At present work, the columns of the AA2300, AA3000 and control series shall

be applied with the Euler column formula.

There are some limitations to the application of the Euler column formula since it is established on the assumption that the column is in a linear elastic state. The stress of the column under compression will not exceed the proportional limit of the material, which shall be described by Equation (26).

$$\sigma_{\mathrm{cr}} = \frac{\pi^2 E}{\lambda^2},\ \sigma_{\mathrm{p}} \tag{26}$$

Where σ_{cr} is the critical stress, λ is the slenderness ratio, σ_p is the proportional limit.

3.4.2 Reduced elastic modulus theory

The Euler column formula does not work for short columns with a height of 600 mm, so reduced modulus theory was adopted to calculate the allowable load of such columns.

When the stress of the column exceeds the proportional limit, the relationship between stress and strain becomes nonlinear. At a level of stress higher than the proportional limit, the tangent slope of the curve may be taken as the elastic modulus at that given stress level, which is typically known as the tangent elastic modulus. However, the elastic modulus of the unloading stage is the same as that of the initial elastic stage. For columns under axial compression whose slenderness ratio is lower than the critical value λ_p, when the stress exceeds the proportional limit, the column transits from unstable straight equilibrium to slightly curved equilibrium. At the compression side of the bending deformation on the section of the component, the compressive stress is higher than $\sigma_{cr} = F_{cr} / A$, the corresponding one at the tension side is lower, as illustrated in Fig. 11b. Furthermore, the tangent elastic modulus should be applied at the compression zone and the unloading elastic modulus at the tension zone. The longitudinal strain at each point of the bending cross section of the column changes linearly along the Y-axis (assuming that the orientation of out of plane bending is parallel to Y-axis). The stresses of the compression and tension zone at the cross section can be obtained by using Equation (27).

$$\left.\begin{array}{ll} \text{Compression zone} & \sigma_c = E_\sigma \dfrac{y}{\rho(x)} \\ \text{Tension zone} & \sigma_t = E \dfrac{y}{\rho(x)} \end{array}\right\} \tag{27}$$

And the stresses acting on the FRP sheet in tension can be obtained by Equation (28).

$$\sigma_f = E_f \frac{y}{\rho(x)} \tag{28}$$

Where $\rho(x)$ is the radius of curvature of the deflection curve.

The position of the neutral axis (which is not identical to the axis of gravity) shall be determined using Equations (29) and (30). Total moment is obtained by integrating over the cross-sectional area as shown in Equations (31) and (32).

$$F_N = \int_A \sigma dA = 0 \tag{29}$$

$$\int_0^{h_1} E_\sigma \frac{y}{\rho(x)} b dy - \int_{h_1-b_1}^{h_1} E_\sigma \frac{y}{\rho(x)} b_1 dy = \int_0^{h_2} E \frac{y}{\rho(x)} b dy - \int_{h_2-b_1}^{h_2} E \frac{y}{\rho(x)} b_1 dy + \int_{h_2}^{h_2+t} E_f \frac{y}{\rho(x)} b dy \tag{30}$$

The magnitudes of the elastic modulus E and the tangent elastic modulus E_σ may be taken as 7782 MPa and 1600 MPa respectively, which were reported by the authors in a previous study [26]. Other parameters are as follows: the width of the section $b = 100$ mm, the height of the section $h = 100$ mm, the width of the chamfers $b_1 = 10$ mm, the thickness and the elastic modulus of the AFRP sheet is 0.2 mm and 165 GPa, respectively. The width of the tensile FRP sheet can be taken as 100 mm for ease of calculation. Once all these parameters are used in Equation (30), the

location of the neutral axis is known as $h_1 = 74.429$ mm and $h_2 = 25.571$ mm.

$$M_z = \int_A y\sigma \, dA = M \tag{31}$$

$$\begin{aligned} M(x) = &\int_0^{h_1} E_\sigma \frac{y^2}{\rho(x)} b dy - \int_{h_1-b_1}^{h_1} E_\sigma \frac{y^2}{\rho(x)} b_1 dy \\ &+ \int_0^{h_2} E \frac{y^2}{\rho(x)} b dy - \int_{h_2-b_1}^{h_2} E \frac{y^2}{\rho(x)} b_1 dy + \int_{h_2}^{h_2+t} E_f \frac{y^2}{\rho(x)} b dy \end{aligned} \tag{32}$$

Once the exact values of all relevant parameters are used, Equation (32) is simplified into Equation (33).

$$M(x) = \frac{1.8858 \times 10^{10}}{\rho(x)} \ \mathrm{N \cdot mm} \tag{33}$$

The relationship between the curvature of the neutral layer $\frac{1}{\rho(x)}$ and the moment is shown as Equation (34).

$$\frac{1}{\rho(x)} = \frac{M(x)}{E_r I} \tag{34}$$

Where is E_r the reduced elastic modulus, which is calculated to be 2387.0886 MPa with I.

Hence, the allowable load of columns with a slenderness ratio lower than λ_p can be predicted using Equation (35), which imitates the Euler column formula.

$$F_{cr} = \frac{\pi^2 E_r I}{l^2} \tag{35}$$

When $\sigma_{cr} > \sigma_p$, the critical stress is:

$$\sigma_{cr} = \frac{\pi^2 E_r}{(\mu l / i)^2} = \frac{\pi^2 E_r}{\lambda^2} \tag{36}$$

While the reduced elastic modulus theory is not applicable to the too-short columns. The critical stress calculated by Equation (36) exceeds the yield stress of the material. For those columns, the yield stress σ_s should be taken as critical stress.

Considering Euler column formula for slender columns and reduced elastic nodulus formula for short columns, the relationship between critical stress and slenderness ratio is shown in Fig. 12.

3.4.3 GB50005-2017 Code for Design of Timber Structures

In the GB50005-2017 [27], the stability factor for columns under axial compression can be calculated by Equations (37) and (38) depending on the strength grade of timber species.

If the strength grade is TC17, TC15 or TB20, the column stability factor φ is given by Equation (37):

$$\varphi = \begin{cases} \dfrac{3000}{\lambda^2}, & \lambda > 75 \\ \dfrac{1}{1 + \left(\dfrac{\lambda}{80}\right)^2}, & \lambda \le 75 \end{cases} \tag{37}$$

If the strength grade is TC11, TC13, TB11, TB13, TB15 or TB17, the column stability factor φ is given by Equation (38):

$$\varphi=\begin{cases}\dfrac{2800}{\lambda^2}, & \lambda>91\\ \dfrac{1}{1+\left(\dfrac{\lambda}{65}\right)^2}, & \lambda\le 91\end{cases} \tag{38}$$

The bearing capacity of the column may be calculated by using Equation (39).

$$P_{\mathrm{ul}}=\varphi f_c A \tag{39}$$

where λ is the slenderness ratio, P_{ul} is the ultimate bearing capacity, f_c is the compressive strength, and A is the section area. The nominal compressive resistance f_c=57.8 MPa is obtained from Zhang et al.'s research [26].

3.4.4 NDS-2018 National Design Specification for Wood Construction

The nominal resistance, P_n, of a component under compression parallel to grain shall be determined using Equation (40) [28]:

$$P_n=F_c^* A C_p \tag{40}$$

Where components are not adequately braced, the nominal stress shall be modified by the column stability factor, C_p, as can be determined using Equations (41), (42) and (43).

$$C_p=\frac{1+\left(F_{cE}/F_c^*\right)}{2c}-\sqrt{\left[\frac{1+\left(F_{cE}/F_c^*\right)}{2c}\right]^2-\frac{F_{cE}/F_c^*}{2c}} \tag{41}$$

$$F_{cE}=\frac{0.822E_{\min}}{\left(l_e/b\right)^2} \tag{42}$$

$$l_e=k_l l \tag{43}$$

If the allowable stress method is adopted, F_c^* may be determined using Equation (44):

$$F_c^*=F_c\times C_D\times C_M\times C_t\times C_i\times C_F \tag{44}$$

In which, F_{cE} is the nominal Euler yield strength, F_c^* is the nominal resistance in compression parallel to the grain. c is the coefficient related to the material, taken as 0.9 when the material is glulam. k_l is the effective length factor, and l_e is the effective length. b is the width of the section. $E_{\min}$ is the elastic modulus. C_M is the wet service factor, which shall be taken as 0.73 for compressive strength and 0.833 for elastic modulus when the environmental humidity is higher than 16%. C_t is the temperature factor, as the experiment was carried out at room temperature, the factor shall be taken as 1.0. C_i is the incising factor, which may be taken as 0.8 for compressive strength and 0.95 for elastic modulus. C_T is the buckling stiffness factor, which is taken as 1.0 conservatively. C_D is the load duration factor, which is taken as 1.0 conservatively. C_F is the load duration factor, which is taken as 1.0 conservatively.

3.4.5 Li et al.'s design model

Li et al. [25] proposed an equation for calculating the stability coefficient φ of laminated bamboo columns as shown in Equation (45):

$$\varphi=0.000106\left(l_0/h\right)^2-0.0298\left(l_0/h\right)+1.1 \tag{45}$$

Here l_0 is the effective length of the laminated bamboo column and h is the height along the eccentric direction of the cross section.

Suppose that the eccentric direction is always along the height orientation of the cross section, then h can be considered as the height of the cross section. The moment of inertia I for a rectangular cross-section can be calculated as Equation (46):

$$I = \frac{bh^3}{12} \tag{46}$$

Using Equations (19) and (20), the relationship between the slenderness ratio and l_0 / h is shown as Equation (47).

$$\lambda = \sqrt{12}\left(l_0 / h\right) \tag{47}$$

Equation (45) can be changed into Equation (48) by using Equation (47), which shows a relationship between the stability coefficient and the slenderness ratio.

$$\varphi = 0.00000883\lambda^2 - 0.0086\lambda + 1.1 \tag{48}$$

It is worth noting that the cross section of the column in Li et al.'s research was in the shape of a rectangle and Equation (48) is not exactly the same as the original one due to the hypothesis.

3.4.6 Tan et al.'s design model

Based on the axial compression test of parallel bamboo strand lumber columns, Tan et al. [29] suggested an equation to predict the ultimate capacity which can be expressed by Equation (49).

$$P = 0.098\lambda^2 - 12.87\lambda + 842.47 \tag{49}$$

The compressive strength of the parallel bamboo strand lumber was 63.92 MPa, and the section area was 10000 mm^2. The relationship between the stability coefficient and the ultimate capacity is shown in Equation (50).

$$\varphi = P / \left(f_c A\right) \tag{50}$$

Then the stability coefficient can be calculated as Equation (51) by using Equation (50):

$$\varphi = 0.00015\lambda^2 - 0.02\lambda + 1.32 \tag{51}$$

3.4.7 Carrying capacity formula of laminated bamboo column under axial compression

The column stability factor for the columns in the current study can be obtained by Formula (50) as shown in Fig. 13.

Results obtained from the current study were used to fit an exponential function and Equation (52) was obtained as the best fit curve as shown in Fig. 13.

$$\varphi = 0.00418e^{\frac{2147.11035}{\lambda + 385.53268}} \tag{52}$$

By substituting Equation (52) into Equation (39), the calculation formula of bearing capacity of the laminated bamboo column with FRP under axial compression with parameters calibrated with experimental data can be obtained. As demonstrated by Table 4 and Fig. 13, the predicted value calculated by the empirical formula is in good agreement with the experimental results, and $R^2 = 0.970$.

The corresponding proposed formula for the bearing capacity of the column is shown as Equation (53):

$$P_{ul} = 2.36772e^{\frac{2147.11035}{\lambda + 385.53268}} \tag{53}$$

3.4.8 Discussion

Table 4 shows comparison of predicted bearing capacities with the relevant test values. Both Euler column formula and reduced elastic modulus theory predictions are conservative. For NDS-2018, predicted values of short columns are higher than the experimental ones, while those for slender columns are conservative. GB50005-2017 consistently overpredicted test resistances but are much more accurate, especially those recommended for TC11 strength group.

Although there are some differences between the calculated values of Li et al.'s model and the experimental ones, the overall trend is quite consistent with the present test results (Fig. 13). Tan et al.'s model is in good agreement with the trend in the previous stage, but the larger slenderness ratio condition does not be fully considered.

Table 4 shows the slenderness ratio of columns, test mean values and ratios of theoretical values to test mean values.

In the equation of the NDS, F_{cE} is the nominal Euler yield strength, which is calculated as $\sigma_{cr}=\frac{\pi^2 E}{\lambda^2}$. In which, the square of the slenderness ratio λ is inversely proportional to the strength, which makes the prediction curve drop fast. If λ^2 is substituted by λ multiplied by a coefficient, such as 50 in the present work. Then F_{cE} shall be $\frac{\pi^2 E}{50\lambda}$, and the curve will be more approximate to the experimental results, as shown in Fig. 14.

4 Conclusion

The aim of the present work was to investigate the feasibility of reinforcing laminated bamboo column by aramid fiber reinforced polymer composites and to examine the effect of slenderness ratio on the ultimate load-carrying capacity, displacement, deflection, and failure mode of such columns. To achieve these outcomes, eighteen full-scale columns were tested under monotonic load in the compression test. Based on the analysis of the test data, the following conclusions can be drawn.

(1) The experimental investigation conducted in this study indicates that AFRP laminates could offer an increase in the strength and stiffness of laminated bamboo columns with even very small area fractions of reinforcement.

(2) It was observed that strain at failure was always significantly smaller than that of wer than the rupture strain of the composite sheets. Therefore, the ultimate strength of AFRP reinforced laminated bamboo column would not be dependent on the tensile strength of fiber composites only, but instead laminated bamboo mechanical properties must always be considered for both ultimate and serviceability limit state designs.

(3) As the slenderness ratio was increased, the load-carrying capacity, the ultimate axial displacement and lateral deflection of columns decreased. Furthermore, the failure modes of short columns vs long columns were distinctly different. The short columns were more prone to strength failure while the slender ones failed in flexural buckling.

(4) Some relevant existing analytical models were used to check their suitability for the considered columns. Obtained test results were used to derive an expression for predicting the stability coefficient φ for AFRP reinforced laminated bamboo columns. The proposed empirical equation produced very good agreement in predicting the ultimate load-carrying capacity.

(5) In addition, column curve proposed by National Design Specification for Wood Construction NDS-2018 was modified to propose another analytical model for considered columns.

The scope of the present study is limited to the results of experimental tests. However, further work still requires to be performed to introduce other parameters such as temperature, and their impact on the performance and structural behavior of fiber composites externally bonded to laminated bamboo columns.

Acknowledgment:

The research work presented in this paper is supported by the Key Laboratory of National Forestry and Grassland Administration/Beijing for Bamboo & Rattan Science and Technology, the National Natural Science Foundation of China (No. 51878354 & 51308301), the Natural Science Foundation of Jiangsu Province (No. BK20181402 & BK20130978), Six talent peak high-level projects of Jiang-su Province (No. JZ-029), and a Project Funded by the Priority Academic Program Development of Jiangsu Higher Education Institutions. Any research results expressed in this paper are those of

the writer(s) and do not necessarily reflect the views of the foundations. The writers gratefully acknowledge Ke Zhou, Hang Li, Chaokun Hong, Dong Yang, Xiaoyan Zheng, Shaoyun Zhu, Liqing Liu, Dunben Sun, Jing Cao, Yanjun Liu and others from the Nanjing Forestry University for helping with the tests.

REFERENCES

[1] Biermann F, Kanie N, Kim RE. Global governance by goal-setting: the novel approach of the UN Sustainable Development Goals. Curr Opin Env Sust 2017;26:26-31.

[2] Xiao Y, Yang RZ, Shan B. Production, environmental impact and mechanical properties of glubam. Constr Build Mater 2013;44:765-73.

[3] Huang D, Bian Y, Zhou A, Sheng B. Experimental study on stress-strain relationships and failure mechanisms of parallel strand bamboo made from phyllostachys. Constr Build Mater 2015;77:130-8.

[4] Li X, Ashraf M, Li H, Zheng X, Wang H, Al-Deen S, Hazell PJ. An experimental investigation on Parallel Bamboo Strand Lumber specimens under quasi static and impact loading. Constr Build Mater 2019;228:116724.

[5] Sun X, He M, Li Z. Novel engineered wood and bamboo composites for structural applications: State-of-art of manufacturing technology and mechanical performance evaluation. Constr Build Mater 2020;249:118751.

[6] Wang Z, Li HT, Lorenzo R, Corbi I, Corbi O, Fang CH. Review on bond properties between wood and fiber reinforced polymer. J Renew Mater 2020;8(8):993-1018.

[7] Plevris N, Triantafillou TC. FRP-reinforced wood as structural material. J Mater Civil Eng ASCE 1992;4(3):300-17.

[8] Sonti S, Davalos JF, Hernandez R, Moody RC, Kim Y. Laminated wood beams reinforced with pultruded fiber-reinforced plastic. In: Proceedings of composites institute's 50th annual conference & Expo'95. Cincinnati, OH: Composites Institute of the Society of the Plastics Industry, Inc., Session 10-B, January 30-February 1, 1995. p.1-5.

[9] Vahedian A, Shrestha R, Crews K. Experimental and analytical investigation on CFRP strengthened glulam laminated timber beams: Full-scale experiments. Compos Part B: Eng 2019;164;377-389.

[10] Wei Y, Ji X, Duan M, Li G. Flexural performance of bamboo scrimber beams strengthened with fiber-reinforced polymer. Constr Build Mater 2017;142:66-82.

[11] Lv QF, Liu Y. Experimental study on the mechanical behavior of BFRP-bamboo composite beam. Adv Compos Lett 2019;28:0963693519867335.

[12] Nugroho N, Ando N. Development of structural composite products made from bamboo II: Fundamental properties of laminated bamboo lumber. J Wood Sci 2001;47(3):237-242.

[13] Mahdavi M, Clouston PL, Arwade SR. Development of laminated bamboo lumber: review of processing, performance, and economical considerations. J Mater in Civil Eng 2011;23(7):1036-42.

[14] Sulaiman O, Hashim R, Wahab R. Evaluation of shear strength of oil treated laminated bamboo. Bioresour Technol 2006;97(18):2466-9.

[15] Li HT, Zhang QS, Huang DS, Deeks AJ. Compressive performance of laminated bamboo. Compos Part B: Eng 2013;54:319-28.

[16] Sharma B, Gatóo A, Ramage MH. Effect of processing methods on the mechanical properties of engineered bamboo. Constr Build Mater 2015;83:95-101.

[17] Xu Q, Chen L, Harries KA, Li X. Combustion performance of engineered bamboo from cone calorimeter tests. Eur J Wood Wood Prod 2017;75(2):161-73.

[18] Xiao Y, Wu Y, Li J, Yang RZ. An experimental study on shear strength of glubam. Constr Build Mater 2017;150:490-500.

[19] Xu M, Cui Z, Tu L, Xia Q, Chen Z. The effect of elevated temperatures on the mechanical properties of laminated bamboo. Constr Build Mater 2019;226:32-43.

[20] Chen G, Yu Y, Li X, He B. Mechanical behavior of laminated bamboo lumber for structural application: an experimental investigation. Eur J Wood Wood Prod 2020;78(1):53-63.

[21] Yu WK, Chung KF, Chan SL. Column buckling of structural bamboo. Eng Struct 2003;25:755-68.

[22] Siddhaye VR, Sonar IP. Behaviour of bamboo under axial compression. J Inst Eng India Civ Eng Div 2006;87(5):3-8.

[23] He M, Li Z, Sun Y, Ma R. Experimental investigations on mechanical properties and column buckling behavior of structural bamboo. The Structural Design of Tall and Special Buildings 2015;24(7):491-503.

[24] Lv XH. Experimental study and finite element analysis of glubam column under axial compression. Chang-sha, China: Thesis of Hu-nan University; 2011.

[25] Li HT, Su JW, Zhang QS, Deeks AJ, Hui D. Mechanical performance of laminated bamboo column under axial compression. Compos Part B: Eng 2015;79:374-82.

[26] Zhang H, Li HT, Hong CK, Lorenzo R, Corbi I, Corbi O. Size effect on the compressive strength of laminated bamboo lumber. (Unpublished results)

[27] GB50005-2017. Code for Design of Timber Structures. Ministry of Housing and Urban-Rural development of the People's Republic of China; 2017.

[28] NDS-2018. Supplement National Design Specification Design Values for Wood Construction. American Forest & Paper Association, American Wood Council; 2018.

[29] Tan C, Li H, Wei D, Lorenzo R, Yuan C. Mechanical performance of parallel bamboo strand lumber columns under axial compression: experimental and numerical investigation. Constr Build Mater 2020;231:117168.

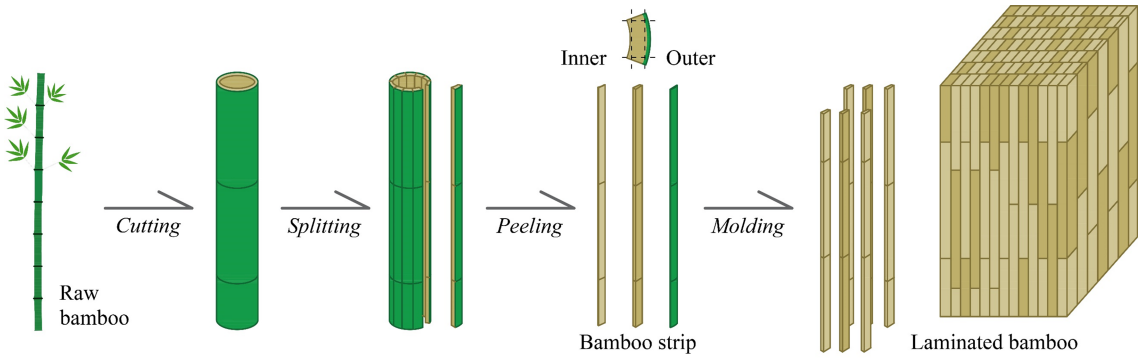

Fig. 1. Schematic diagram of manufacturing process of laminated bamboo

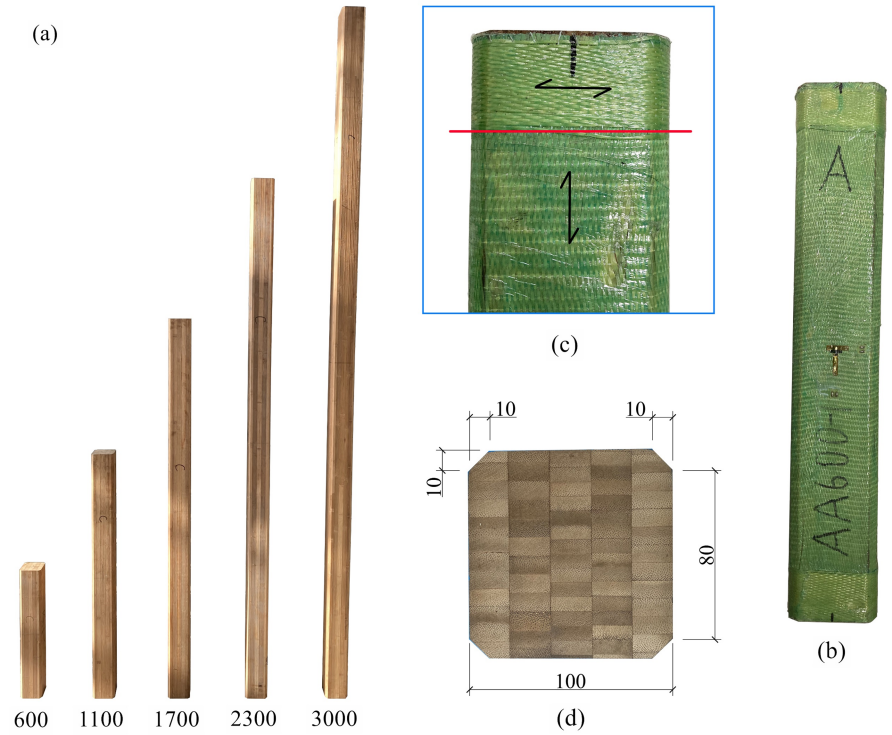

Fig. 2 Laminated bamboo column and wrapped aramid fiber reinforced polymer: (a) specimens with different slenderness ratio, (b) column reinforced with AFRP, (c) extra reinforcement at the end of the column, and (d) the cross-section of the column. All dimensions are in mm

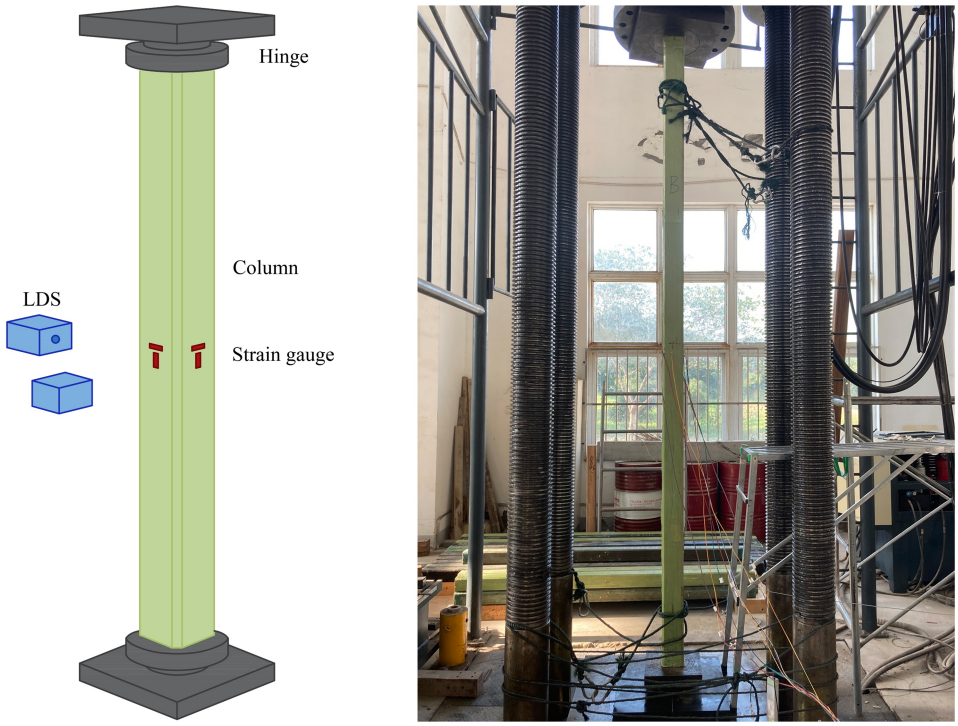

(a) (b)

Fig. 3 Setup used for compression tests (a) schematic and (b) physical

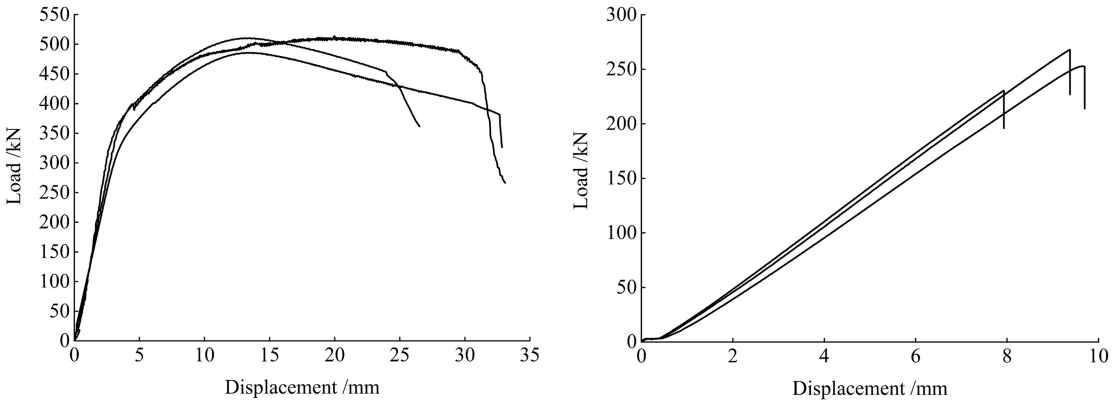

(a) AA600 (b) AA3000

Fig. 4 Load-displacement curves of (a) AA600 series and (b) AA3000 series

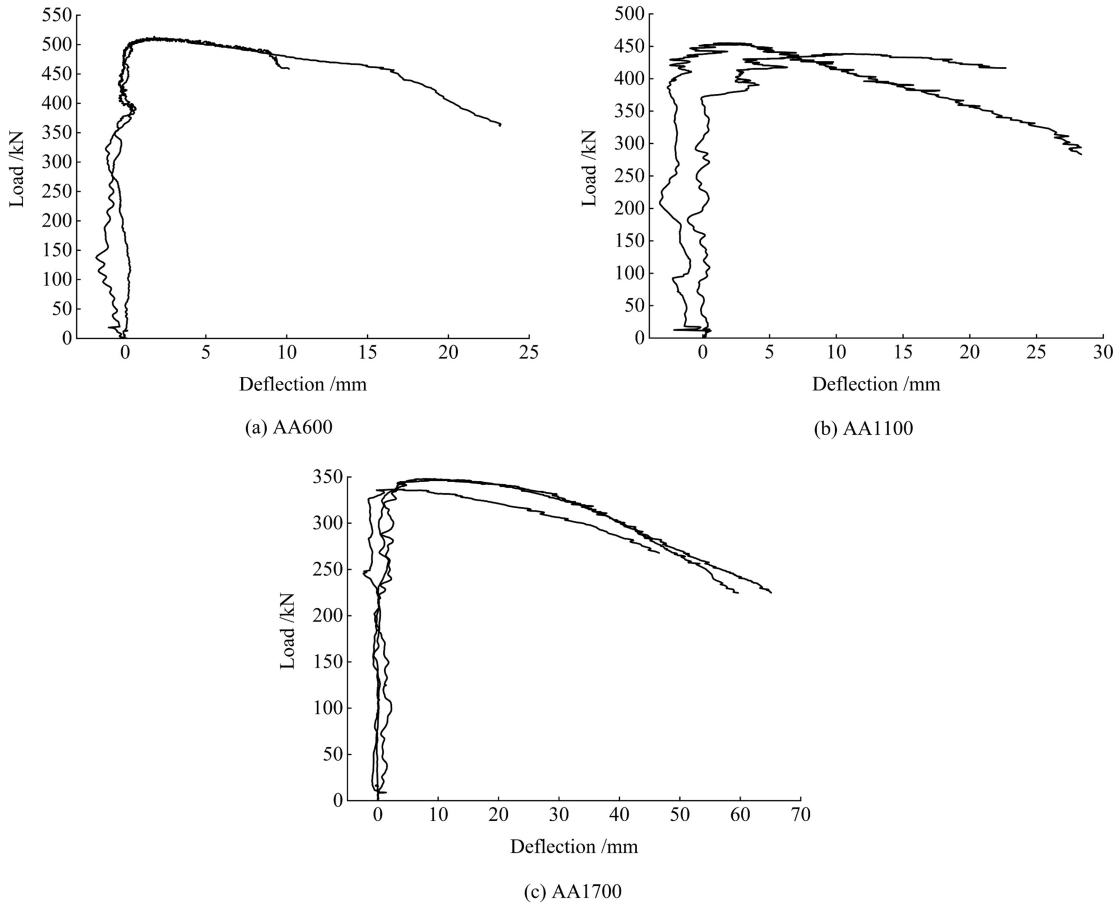

Fig. 5 Load-deflection behaviors of AA600, AA1100, and AA1700 series

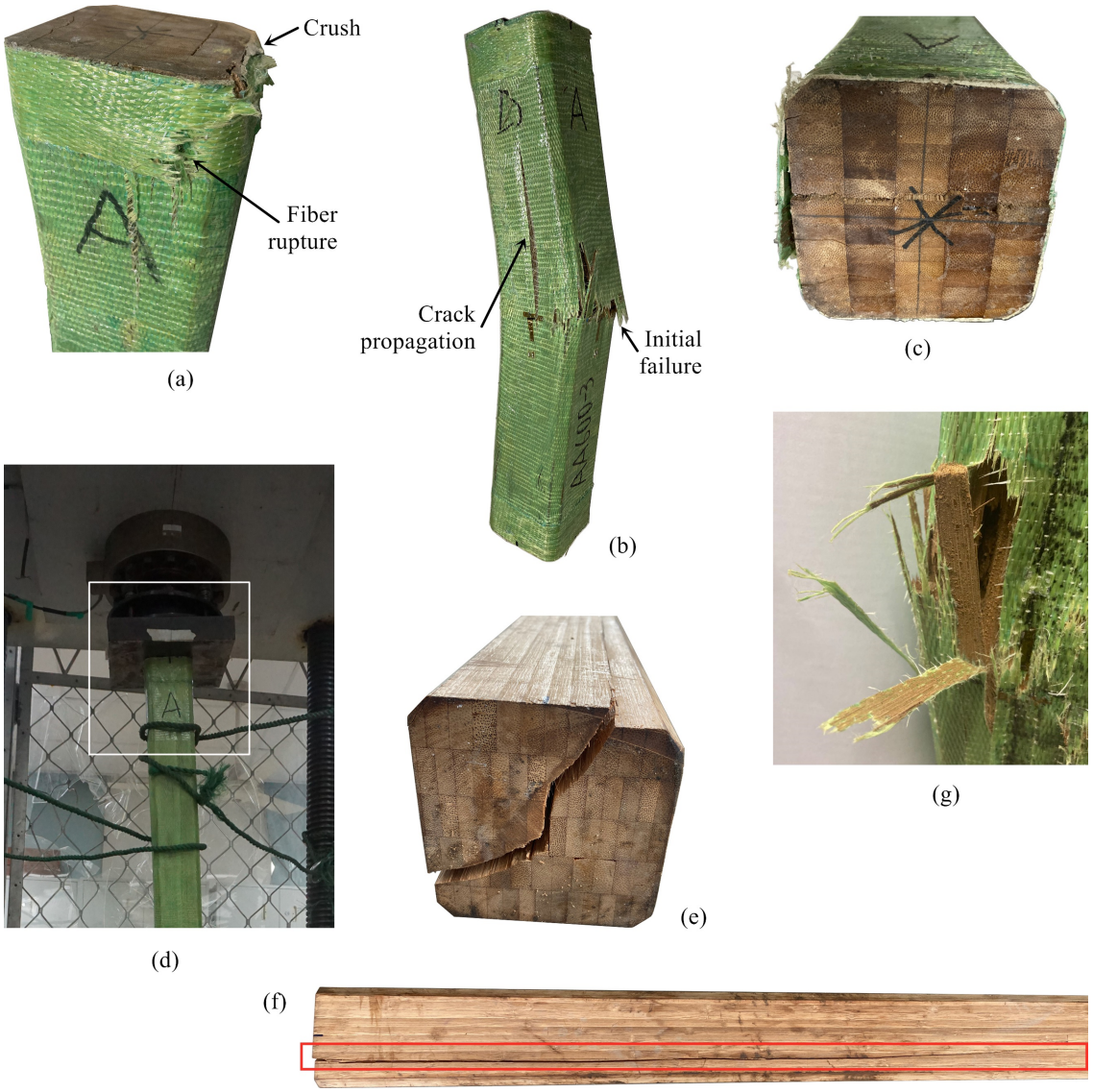

Fig. 6 Failure phenomena: (a) end crush of AA600-2, (b) AA600-3, (c) cracks of the AA600-3 end, (d)hinge tilted, (e) crack of the Control-1 end, (f) splitting extending to the middle of the Control-1 specimen, and (g) debonding of composite sheet and traces of bamboo showing strong bonding between AFRP and bamboo

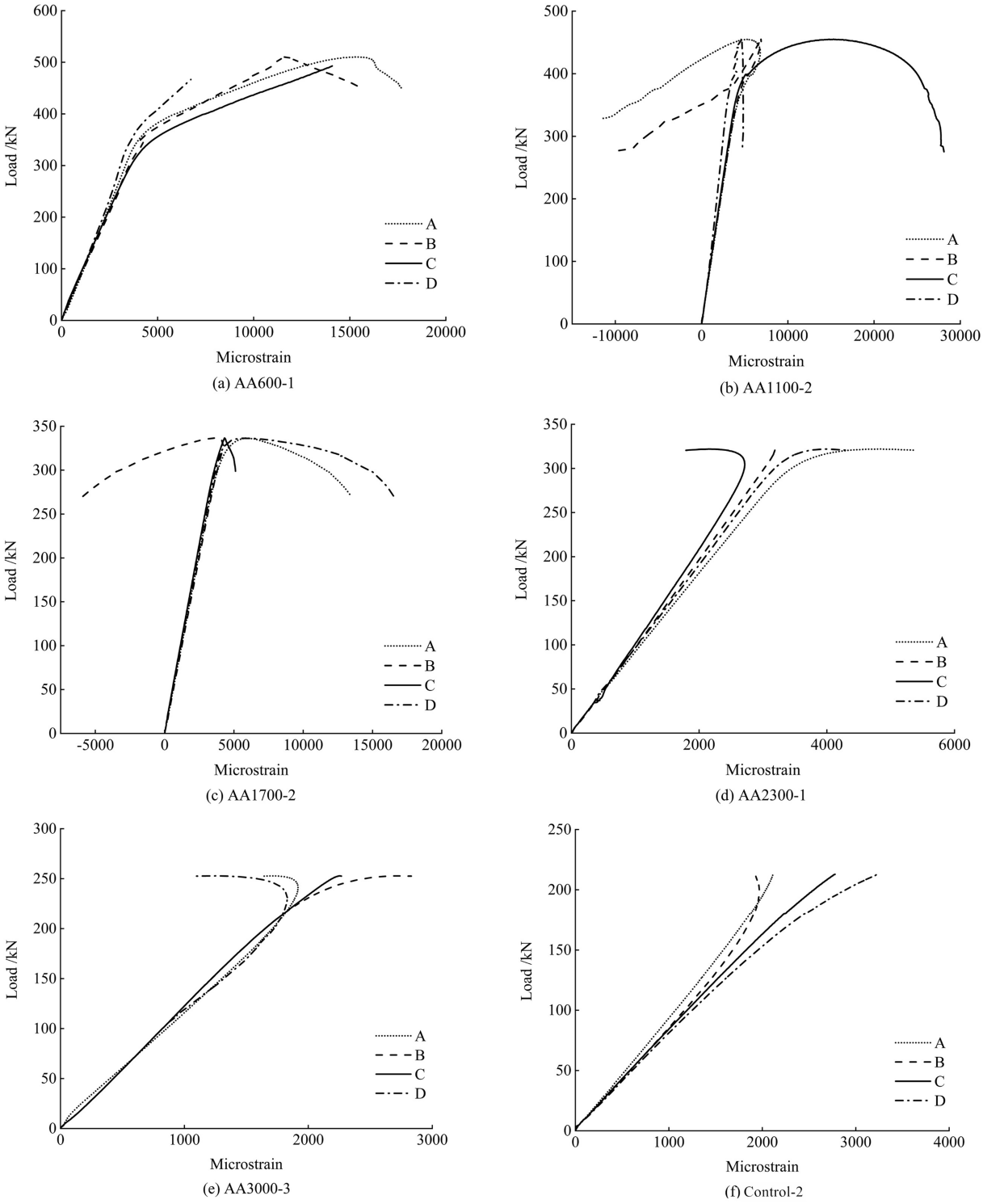

Fig. 7 Load-strain behaviors

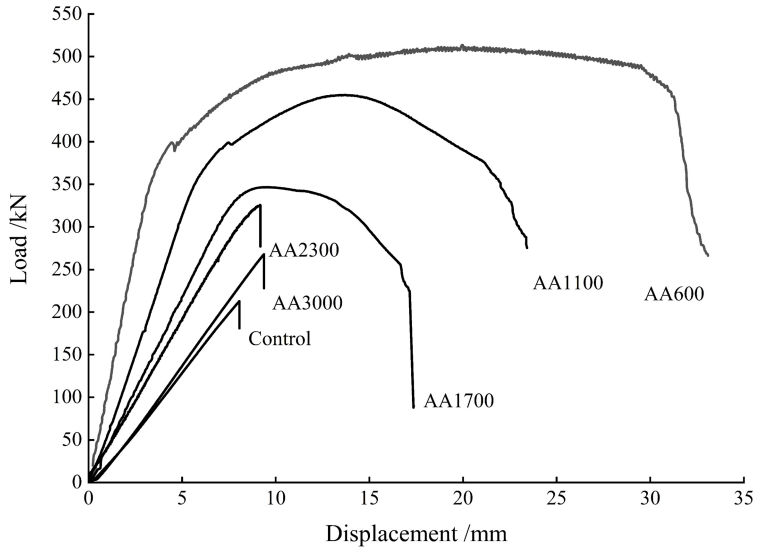

Fig. 8 Comparison of load-displacement behaviors

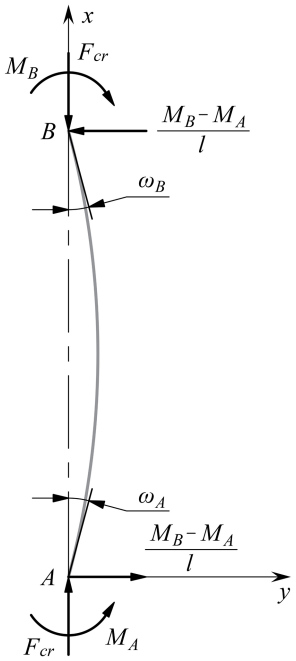

Fig. 9 Calculation diagram of a column

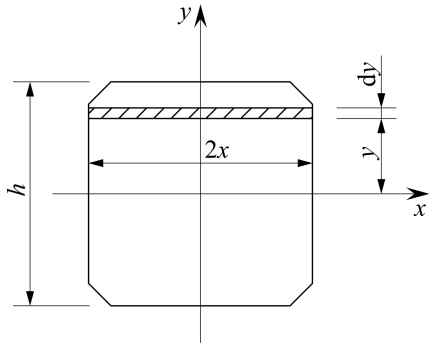

Fig. 10 Moment of inertia of the column section including cambers

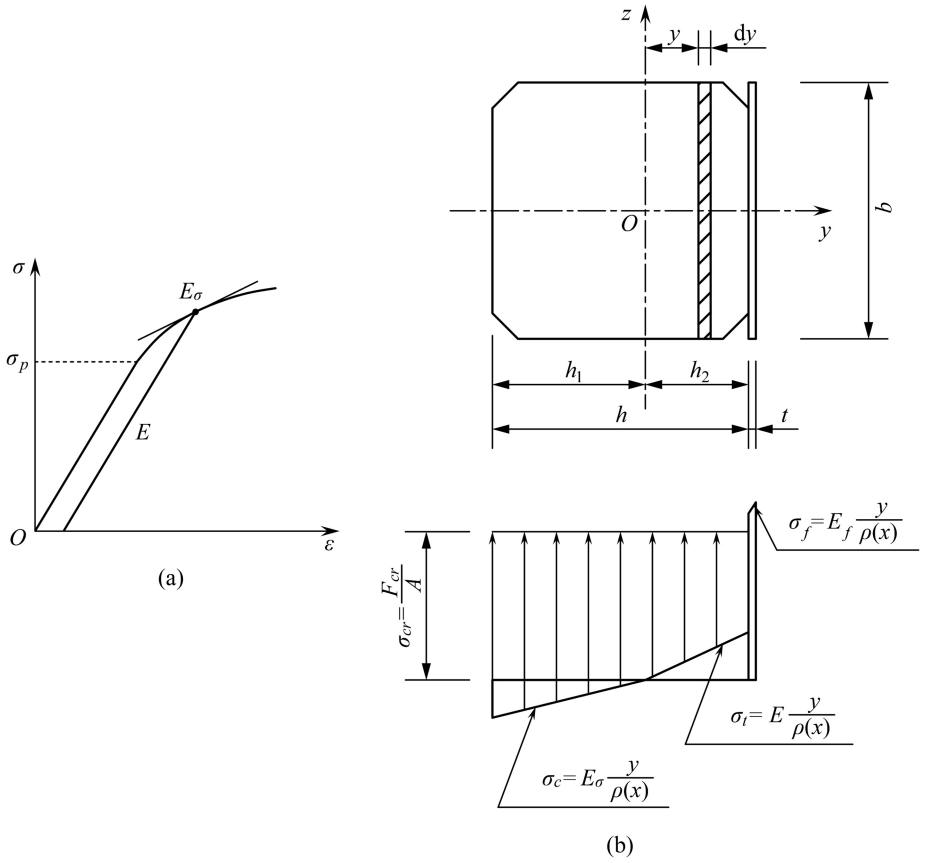

Fig. 11 Calculation diagram of bending moment

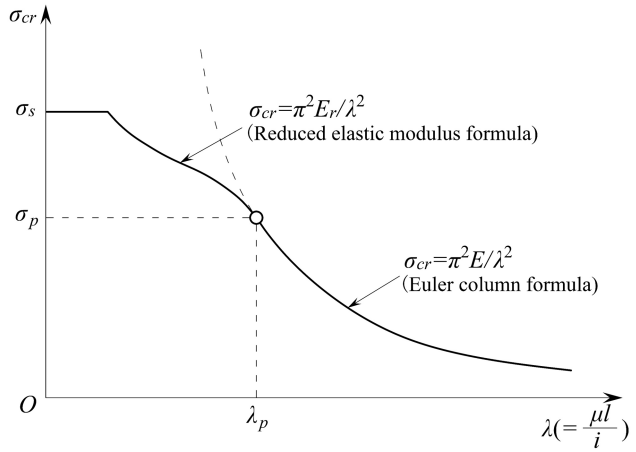

Fig. 12 Relationship between critical stress and slenderness ratio of Euler column formula and reduced elastic nodulus formula

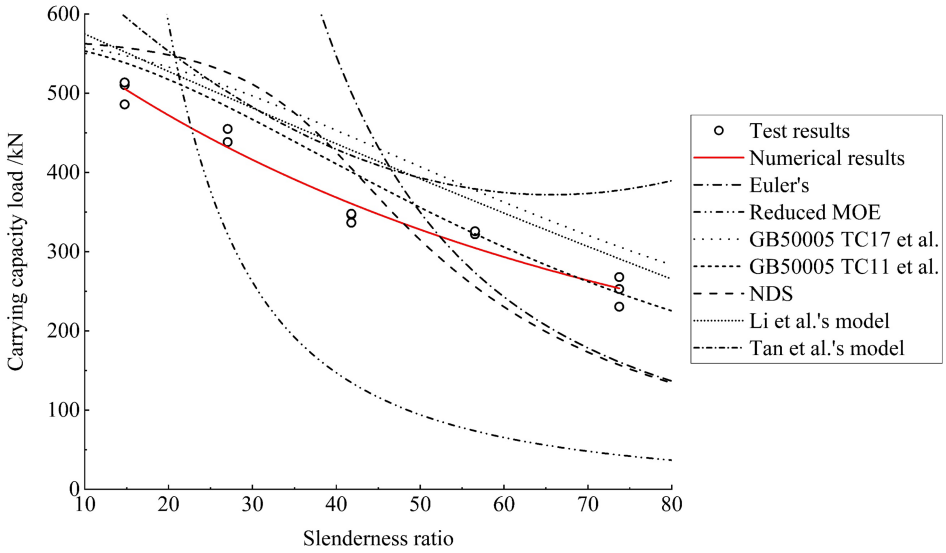

Fig. 13 Comparison of test results with various analytical models and the proposed equation

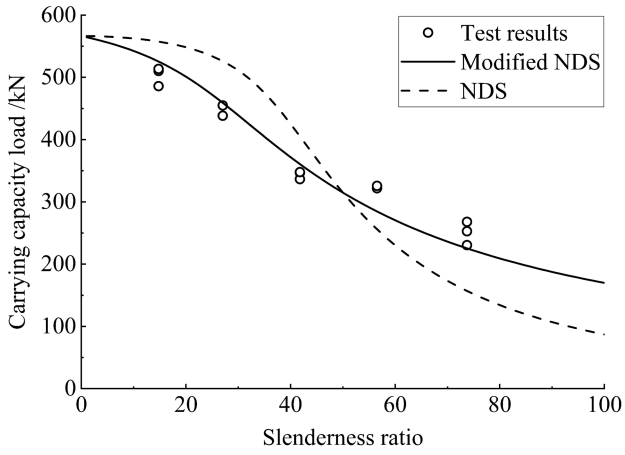

Fig. 14 Modified NDS prediction curve

Table 1 Geometric details of the specimen groups used in testing program

Series	Fiber	Volume fraction of AFRP (%)	No. of specimens	Length (mm)
AA600	Aramid	0.77	3	600
AA1100	Aramid	0.77	3	1100
AA1700	Aramid	0.77	3	1700
AA2300	Aramid	0.77	3	2300
AA3000	Aramid	0.77	3	3000
Control	--	--	3	3000

Table 2 Details of tests results

Series	Ultimate load (kN)	Axial displacement (mm)	Compressive strength (MPa)	Stiffness (kN/mm)	Volume fraction of reinforcement (%)
Control-1	225.9	8.8	23.1	27.3	--
Control-2	212.8	8.1	21.7	27.5	--
Control-3	225.7	9.1	23.0	25.6	--
Mean	221.5	8.7	22.6	26.8	
COV	3.4%	6.2%	3.4%	3.8%	
AA3000-1	230.4	7.9	23.5	30.6	0.77
AA3000-2	267.9	9.4	27.3	29.9	0.77
AA3000-3	252.8	9.6	25.8	28.0	0.77
Mean	250.4	9.0	25.6	29.5	
COV	7.5%	10.3%	7.5%	4.5%	
Enhancement			13.1%	10.0%	

Note: COV means the coefficient of variation. Enhancement of strength or stiffness is the increment of columns with FRP based on the mean value for the Control series.

Table 3 Details of tests results

Series	Ultimate load (kN)	Axial displacement (mm)	Compressive strength (MPa)	Vertical ultimate strain	Horizontal ultimate strain
AA600-1	510.4	13.2	52.1	11599	5068
AA600-2	513.6	20.0	52.4	11199	5032
AA600-3	485.9	13.4	49.6	--	--
Mean	503.3	15.5	51.4	11399	5050
COV	3.0%	25.0%	3.0%	2.5%	0.5%
AA1100-1	438.5	13.3	44.7	6639	2640
AA1100-2	454.9	13.5	46.4	7970	3318
AA1100-3	--	--	--	--	--
Mean	446.7	13.4	45.6	7304	2979
COV	2.6%	0.9%	2.6%	12.9%	16.1%
AA1700-1	346.9	9.6	35.4	5511	1759
AA1700-2	336.6	9.6	34.3	4903	1425
AA1700-3	348.0	9.5	35.5	4790	1139
Mean	343.8	9.6	35.1	5068	1441
COV	1.8%	0.5%	1.8%	7.7%	21.5%
AA2300-1	321.9	12.0	32.8	3456	1083
AA2300-2	325.7	9.1	33.2	3987	1040
AA2300-3	--	--	--	--	--
Mean	323.8	10.6	33.0	3722	1062
COV	0.8%	19.7%	0.8%	10.1%	2.9%
AA3000-1	230.4	7.9	23.5	1511	579
AA3000-2	267.9	9.4	27.3	2682	648
AA3000-3	252.8	9.6	25.8	2501	644
Mean	250.4	9.0	25.6	2232	624
COV	7.5%	10.3%	7.5%	28.2	6.2%

Note: The strain data of AA600-3 was lost and the tests of AA1100-3 and AA2300-3 were terminated due to unforeseen technical issues.

Table 4 Comparison between test value and calculated value

	AA600	AA1100	AA1700	AA2300	AA3000	Control
Slenderness ratio	14.7	26.9	41.6	56.2	73.3	74.0
Test mean value (kN)	503.3	446.7	343.8	323.8	250.4	221.5
Euler column formula	--	--	--	0.74	0.56	0.62
Reduced elastic modulus theory	2.09	0.70	0.38	--	--	--
GB50005-2017 (TC17 strength group)	1.09	1.14	1.30	1.17	1.23	1.38
GB50005-2017 (TC11 strength group)	1.07	1.08	1.17	1.00	1.00	1.11
NDS-2018	1.09	1.14	1.06	0.68	0.54	0.59
Modified NDS equation	1.04	1.03	1.05	0.88	0.90	1.01
Proposed formula (53)	1.01	0.97	1.05	0.94	1.02	--